

Synthesis and structural characterization of perovskite YFeO_3 by thermal decomposition of a cyano complex precursor, $\text{Y}[\text{Fe}(\text{CN})_6] \cdot 4\text{H}_2\text{O}$

Diego M. Gil · M. Carolina Navarro ·
M. Cristina Lagarrigue · J. Guimpel ·
Raúl E. Carbonio · M. Inés Gómez

Received: 2 September 2010 / Accepted: 8 November 2010 / Published online: 15 December 2010
© Akadémiai Kiadó, Budapest, Hungary 2010

Abstract The thermal decomposition of $\text{Y}[\text{Fe}(\text{CN})_6] \cdot 4\text{H}_2\text{O}$ has been studied in order to investigate the formation of the multi-ferroic oxide YFeO_3 . The starting material ($\text{Y}[\text{Fe}(\text{CN})_6] \cdot 4\text{H}_2\text{O}$) and the decomposition products were characterized by IR spectroscopy, thermal analysis, X-ray powder diffraction (PXRD), and scanning electron microscopy. Metastable YFeO_3 with hexagonal structure, space group $P6_3/mmc$, was obtained by thermal decomposition of $\text{Y}[\text{Fe}(\text{CN})_6] \cdot 4\text{H}_2\text{O}$ at 600 °C in air. Orthorhombic YFeO_3 was obtained by the same method at $T \geq 800$ °C in air. The crystal structure of orthorhombic YFeO_3 was refined by Rietveld analysis using PXRD data. We found that it was slightly deficient in Y^{3+} , which is in agreement with the small amount of Y_2O_3 found as impurity in the sample. The formula of the orthorhombic phase is $\text{Y}_{0.986}\text{FeO}_3$.

Keywords $\text{Y}[\text{Fe}(\text{CN})_6] \cdot 4\text{H}_2\text{O} \cdot \text{YFeO}_3$ · Crystal structure · Low temperature synthesis · Thermal decomposition

Introduction

Multi-ferroics are materials that are magnetically ordered, being at the same time in a ferroelectric state. The coupling between the electric and magnetic polarizations, i.e., the magnetoelectric effect, imparts great value to such materials for practical applications due to the possibility of controlling the magnetic polarization by an electric field and vice versa [1]. We can find many examples of these materials in the perovskite-type oxides family, i.e., BiFeO_3 , BiMnO_3 , YMnO_3 , YCrO_3 , and YFeO_3 [2–7]. Yttrium orthoferrite, YFeO_3 , has a distorted perovskite structure, exhibits a weak ferromagnetic behavior, and shows an antiferromagnetic nature with a high-Néel temperature T_N around 640 K [6, 7]. YFeO_3 crystallizes in either orthorhombic perovskite or hexagonal (YAlO_3 -type) structures, depending of synthesis conditions [8–10]. The stable high temperature phase adopts the orthorhombic perovskite structure, space group $Pnma$, as shown by synchrotron X-ray and neutron diffraction studies [10]. The metastable low-temperature compound with hexagonal structure has been studied by X-ray and neutron diffraction for the palladium-doped compound, $\text{YFe}_{1-x}\text{Pd}_x\text{O}_{3-\delta}$ [11].

The orthoferrite YFeO_3 has been widely studied for its magnetic and magneto-optical properties [6, 7, 9], and used in gas sensors [12, 13], environmental monitoring applications [14], and catalysis [11]. YFeO_3 -based catalysts have been explored only for photocatalytic oxidation of organic dyes [9, 15] and the selective catalytic reduction of NO_x to N_2 by propene under lean conditions [16, 17].

J. Guimpel and Raúl E. Carbonio are members of the Research Career of CONICET.

D. M. Gil · M. C. Navarro · M. C. Lagarrigue ·
M. I. Gómez (✉)

Instituto de Química Inorgánica, Facultad de Bioquímica,
Química y Farmacia, Universidad Nacional de Tucumán,
Ayacucho 471, 4000 San Miguel de Tucumán, Argentina
e-mail: mgomez@fbqf.unt.edu.ar

R. E. Carbonio
Departamento de Fisicoquímica, Facultad de Ciencias Químicas,
Instituto de Investigaciones en Fisicoquímica de Córdoba
(INFIQC)-CONICET, Universidad Nacional de Córdoba,
Ciudad Universitaria, X5000HUA Córdoba, Argentina

J. Guimpel
Centro Atómico Bariloche, Instituto Balseiro, Comisión
Nacional de Energía Atómica, Universidad Nacional de Cuyo,
8400 San Carlos de Bariloche, Argentina

Li et al. have found that hexagonal YFeO_3 has a high-catalytic activity for the CO oxidation [11].

Several methods for the synthesis of YFeO_3 were informed. Preparation of single phase yttrium orthoferrite by conventional solid state reaction of precursors oxides is difficult due to the preferred formation of secondary phases like $\text{Y}_3\text{Fe}_5\text{O}_{12}$ (yttrium-iron garnet) and Fe_3O_4 [7, 10, 18, 19]. Other synthesis routes have also been proposed including sol-gel processing of a Y-Fe mixed-metal alkoxide [6, 8, 20], Pechini method [11, 21], microwave-assisted synthesis [15], mechanochemically assisted synthesis [22], self-propagating combustion synthesis [9, 23], and inductively coupled plasma [24].

Heteronuclear complexes of the type $\text{A}[\text{MM}'(\text{CN})_6] \cdot n\text{H}_2\text{O}$ (A = lanthanide, alkaline earth metal, Pb or Bi; M, M' = transition metals) have been extensively studied as precursors for perovskite-type oxides $\text{AMM}'\text{O}_{3-\delta}$. The decomposition of the heteronuclear hexacyano-complexes is a promising method for the preparation of homogeneous mixed oxides on an atomic level at low temperatures compared with the conventional ceramic method [25–36]. These oxides have relatively high specific surface areas and thus can be used as catalysts in different reactions [30].

Gómez et al. proposed the synthesis of high surface area perovskites $\text{AFeO}_{3-\delta}$ (A is alkaline earth metal) by thermal decomposition of alkaline earth nitroprussides ($\text{A}[\text{Fe}(\text{CN})_5\text{NO}] \cdot n\text{H}_2\text{O}$) at low temperature, with a high content of Fe(IV) [35, 36].

Some perovskites like LaCrO_3 and LaCoO_3 were obtained by thermal decomposition of $\text{La}[\text{Cr}(\text{C}_2\text{O}_4)_3] \cdot 9\text{H}_2\text{O}$ and $\text{La}[\text{Co}(\text{C}_2\text{O}_4)_3]8 \cdot 5\text{H}_2\text{O}$, respectively [37, 38].

In this article, we propose the synthesis of YFeO_3 obtained by thermal decomposition of $\text{Y}[\text{Fe}(\text{CN})_6] \cdot 4\text{H}_2\text{O}$ and its structural characterization. We refine the crystal structure of YFeO_3 using conventional X-ray powder diffraction (PXRD) by Rietveld Analysis. We also follow the decomposition process through IR spectroscopy, thermogravimetric, and differential thermal analysis (TG and DTA) and PXRD. The size and morphology of the particles were determined by scanning electron microscopy (SEM), and the chemical composition was determined by energy-dispersive spectroscopy (EDS) analyzer. The magnetic properties of orthorhombic YFeO_3 have been investigated.

Experimental

Preparation of $\text{Y}[\text{Fe}(\text{CN})_6] \cdot 4\text{H}_2\text{O}$ precursor

The heteronuclear complex $\text{Y}[\text{Fe}(\text{CN})_6] \cdot 4\text{H}_2\text{O}$ was synthesized by mixing aqueous solutions of equimolar amounts of $\text{K}_3[\text{Fe}(\text{CN})_6]$ and $\text{Y}(\text{NO}_3)_3 \cdot 6\text{H}_2\text{O}$ (prepared from the evaporation of a solution of concentrated HNO_3 and Y_2O_3)

under continuous stirring at 60 °C for 2 h. The resulting orange precipitate was separated by filtration, washed with water and ethanol, and finally stored in the dark in a dry box with silica gel.

Preparation of YFeO_3 perovskite

YFeO_3 was prepared by heating $\text{Y}[\text{Fe}(\text{CN})_6] \cdot 4\text{H}_2\text{O}$ for 6 h at different temperatures (in the range from 600 to 950 °C) in air. The sample was introduced into the furnace and heated from room temperature at 5 °C/min to the desired temperature where it was maintained for 6 h. After that, it was cooled to room temperature at 5 °C/min.

Characterization

Thermogravimetric and differential thermal analysis curves were performed in a Shimadzu TGA/DTA-50 in the temperature range from 20 to 800 °C at a heating rate of 5 °C/min under flowing air.

Infrared spectra (in the region of 4,000–400 cm^{-1}) were recorded at room temperature (RT) on a FTIR Perkin Elmer 1600 spectrophotometer in the transmission mode using KBr pellets.

PXRD profiles were obtained at RT in an X-Pert Pro PANalyticals diffractometer with Cu K_α radiation $\lambda = 1.5418 \text{ \AA}$, between 5° and 120° in 2θ in steps of 0.02° and step time of 10 s. The refinement of the crystal structures was performed by means of the Rietveld method [39] using the FULLPROF program [40]. The structural refinement of YFeO_3 was performed in the space group $Pnma$, with the initial structural model [10]. A pseudo-Voigt function convoluted with an axial divergence asymmetry function was chosen to generate the peak shapes [41].

The size and morphology of the particles were determined by SEM (ZEIS SUPRA-55 VP), and the chemical compositions in the powders were determined with an Oxford INCA PentaFet X3 energy dispersive X-ray analyzer.

The magnetic measurements in the temperature range 5–300 K were performed with a Superconducting Quantum Design Interference Device (SQUID). The magnetization values were measured under zero field cooling (ZFC) and field cooling (FC) conditions at an applied magnetic field of 5 T.

Results and discussion

$\text{Y}[\text{Fe}(\text{CN})_6] \cdot 4\text{H}_2\text{O}$

Figure 1 shows the TG and DTA curves for the thermal decomposition of $\text{Y}[\text{Fe}(\text{CN})_6] \cdot 4\text{H}_2\text{O}$ in air. The first step

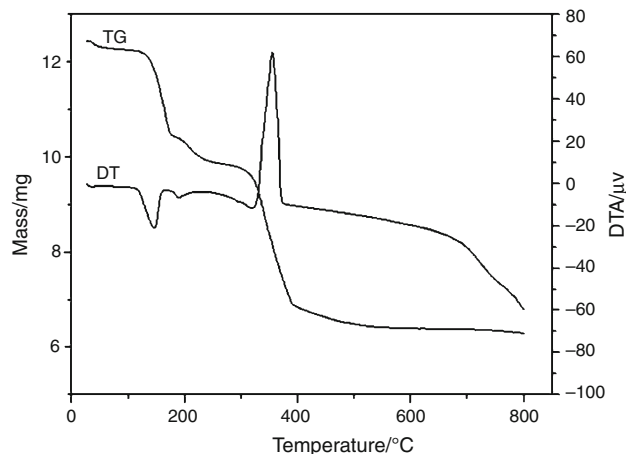
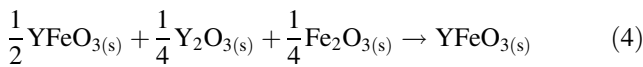
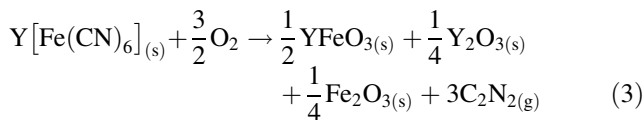
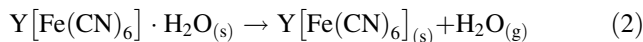
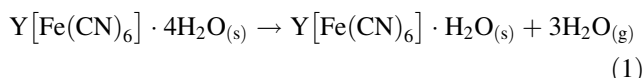


Fig. 1 TG and DTA curves for Y[Fe(CN)₆]·4H₂O in air

corresponds to the loss of three molecules of water and the second one to the loss of the remaining water molecule. These processes suggest that there are two different kinds of water molecules, as was deduced from the crystal structure and FTIR analysis (see below). The third step occurs in the temperature range 265–650 °C, which corresponds to the elimination and oxidation of the cyanide groups with the simultaneous formation of simple oxides (Y₂O₃, Fe₂O₃) and mixed oxide (YFeO₃). In the last step, the simple oxides react to produce the mixed oxide YFeO₃.

The sequence of decomposition steps could be expressed as:



The mechanism of thermal decomposition of ferricyanides has been previously studied by several authors [42–44]. Most of them propose for the decomposition under vacuum, the formation of ferrocyanide as an intermediate product, and the reaction produces gas cyanogen. In this case, the thermal decomposition was carried out in air, therefore is not expected Fe reduction and the formation of ferrocyanide due to the oxidative atmosphere, so that the residues were single and mixed oxides. This is in agreement with Gallagher et al., who have studied the thermal decomposition of europium ferricyanide in air and under vacuum. For pyrolysis in air, they propose the formation of mixture of oxides Eu₂O₃ and α-Fe₂O₃ that at higher temperatures transforms to EuFeO₃ [45].

Table 1 Steps for the thermal decomposition of Y[Fe(CN)₆]·4H₂O and % of mass loss

Steps	Temperature range/°C	Theoretical mass loss/%	Observed mass loss/%
1	60–175	14.49	14.94
2	175–265	4.83	4.75
3	265–650	28.96	28.42
4	>650	—	—
Total mass loss/%		48.28	48.11

The mass losses expected in each of the decomposition steps are in good agreement with those calculated from TG curve. These results are shown in Table 1. Solid residues obtained in the third stage of the process have been confirmed from PXRD and FTIR. At temperatures higher than 650 °C, the mass remained constant and the simple oxides react to produce YFeO₃ (step 4).

The total mass loss from room temperature to 650 °C is 48.11%. It is in agreement with the theoretical mass loss (48.28%) for the formation of YFeO₃ from the complex. The DTA curve shows two endothermic peaks, at 142 and 187 °C, both due to dehydration. The third exothermic peak located at 359 °C corresponds to the elimination and oxidation of the cyanide groups. The fourth step is not observed in DTA since the energy involved in the process is much weaker than the other steps.

The FTIR spectrum of Y[Fe(CN)₆]·4H₂O is shown in Fig. 2. The IR spectra of hexacyanometallates are composed of three vibrations within the octahedral unit M(CN)₆: ν(CN), δ(MCN), and ν(MC); and those motions from crystal water, ν(OH), and δ(HOH) when it is present [46]. For Y[Fe(CN)₆]·4H₂O, antisymmetric and symmetric ν(CN) stretching bands are observed at 2,152 and 2,142 cm⁻¹, respectively. For the bending vibrations of water at least three bands are well resolved. The highest frequency band in the δ(HOH) region, at 1,680 cm⁻¹, corresponds to the weakly bonded waters, the intermediate one at 1,640 cm⁻¹ also belongs to coordinated water molecules but with a weaker coordination bond, and the band at 1,610 cm⁻¹ is attributed to those water molecules with the strong interaction with Y³⁺. In the water stretching region (3,700–3,200 cm⁻¹), bands appear due to coordinated and hydrogen-bonded water with vibrational overtones. The bands at 600–400 cm⁻¹ are related to the vibrations of Fe–CN bonds [46, 47].

YFeO₃ obtained by thermal decomposition of Y[Fe(CN)₆]·4H₂O

In order to obtain a pure phase of the mixed oxide, thermal treatments in air atmosphere at different temperatures were

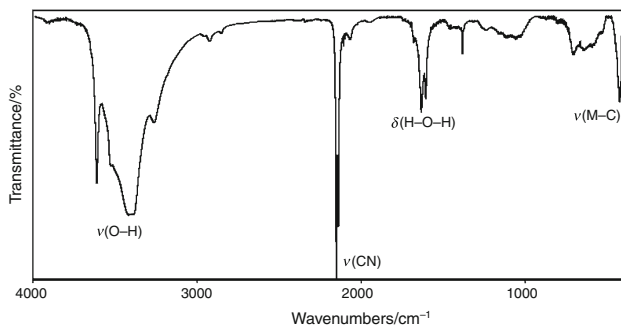


Fig. 2 FTIR spectra of $\text{Y}[\text{Fe}(\text{CN})_6] \cdot 4\text{H}_2\text{O}$

carried out. The resulting products in each stage were characterized by PXRD (see Fig. 3). The composition of the residues at different temperatures was determined using X'Pert Highscore Program (version 2.1b, produced by PANalytical B.V. Almelo, Netherland). When the complex was decomposed at 650 and 700 °C, some peaks attributed to hexagonal YFeO_3 (PDF # 48-529) together with Fe_2O_3 and Y_2O_3 were observed, showing an incomplete reaction.

The crystal structure of hexagonal YFeO_3 (space group $P6_3/mmc$) is similar to that of hexagonal YAlO_3 . It consists of alternating layers of corner-sharing FeO_5 trigonal bipyramids and planes of Y. Each Y atom can be described as sitting at the center of an edge-sharing octahedron formed by closed-packed oxygens, with two additional face-capping oxygens, at longer distances [11].

When the complex was treated at 750 °C, a mixture of hexagonal YFeO_3 and orthorhombic YFeO_3 (PDF # 86-171) were observed. When we increase the temperature ($T > 800$ °C), orthorhombic YFeO_3 with a small amount of Y_2O_3 were formed. Thus, using this preparation method, we were able to prepare YFeO_3 with two different crystal structures, the hexagonal one at $T \approx 650\text{--}700$ °C and the orthorhombic one at higher temperatures ($T > 800$ °C).

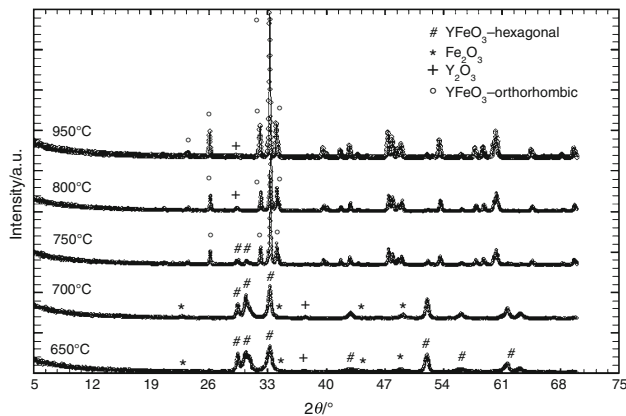


Fig. 3 PXRD data of samples obtained by thermal decomposition of $\text{Y}[\text{Fe}(\text{CN})_6] \cdot 4\text{H}_2\text{O}$ at 650, 700, 750, 800, and 950 °C

The orthorhombic structure in perovskite phase is thermodynamically stable for all lanthanides. The hexagonal structure may exist in a metastable phase for some lanthanides depending on ionic radii. Wu et al. reported the synthesis of YFeO_3 hexagonal and orthorhombic by self-propagating combustion [9].

The use of a precursor containing the appropriate Y/Fe ratio enforces the formation of YFeO_3 with the precise stoichiometry thus controlling and preventing any elements segregation generally observed in conventional methods and allowing to obtain the desired mixed oxide at very low temperatures.

The refined PXRD data taken at room temperature for YFeO_3 prepared by thermal decomposition of $\text{Y}[\text{Fe}(\text{CN})_6] \cdot 4\text{H}_2\text{O}$ at 950 °C in air are shown in Fig. 4. Rietveld structure refinement of YFeO_3 was performed in the space group $Pnma$ using as structural model, the structure informed in ICSD #80865. Some evidence for unreacted Y_2O_3 was seen in the diffraction data, because of this, vacancies on the yttrium site in YFeO_3 were also refined. We obtained an occupancy of 0.986(1) for Y^{3+} , which indicates that some Fe^{3+} should be oxidized to Fe^{4+} . Results for the complete structural refinement for YFeO_3 prepared at 950 °C are shown in Table 2.

The structure of YFeO_3 is very similar to that of the rare earth orthoferrites such as GdFeO_3 with a distorted perovskite-type structure. YFeO_3 perovskite has an yttrium-deficient structure and we can write the formula as $\text{Y}_{0.986}\text{FeO}_3$.

In an ideal (cubic) perovskite structure ABO_3 , the large A cation is surrounded by 12 oxygens, whereas the smaller B cation is in oxygen octahedral coordination. The iron-centered octahedra in YFeO_3 are not ideal. In the structure of YFeO_3 , the coordination of Y^{3+} is reduced from 12 to 8

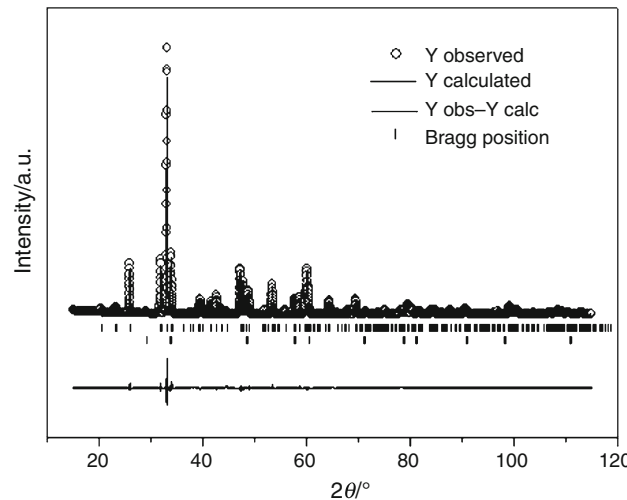


Fig. 4 Rietveld analysis of PXRD data for YFeO_3 obtained by thermal decomposition of $\text{Y}[\text{Fe}(\text{CN})_6] \cdot 4\text{H}_2\text{O}$ at 950 °C

Table 2 Crystallographic parameters for YFeO_3 obtained by thermal decomposition of $\text{Y}[\text{Fe}(\text{CN})_6] \cdot 4\text{H}_2\text{O}$ at 950 °C, after Rietveld refinement with PXRD data

Atom	Wyckoff site	x	y	z	Occupancy
Fe	4b	0	0	0.5	1.0
Y	4c	0.06854 (5)	0.25	0.98218 (7)	0.986 (1)
O1	4c	0.4623 (4)	0.25	0.1120 (4)	1.0
O2	8d	0.6948 (3)	-0.0563 (2)	0.3088 (3)	1.0

Space group: $Pnma$; cell parameters: $a = 5.5941(1)\text{\AA}$, $b = 7.6035(1)\text{\AA}$, $c = 5.2802(1)\text{\AA}$, $V = 224.59(1)$, $Z = 4$

Discrepancy factors: $R_{wp} = 10.8$, $R_{exp} = 5.10$, $\chi^2 = 4.46$, $R_{Bragg} = 2.51$, $R_p = 8.06$

Weight fraction of $\text{Y}_2\text{O}_3 = 1.45\%$

oxygens. The Y^{3+} ion is too small to be fully coordinated by 12 oxygens as required in an ideal perovskite structure.

IR spectra for the samples obtained by thermal decomposition of $\text{Y}[\text{Fe}(\text{CN})_6] \cdot 4\text{H}_2\text{O}$ at different temperatures are shown in Fig. 5. Two absorption peaks are present in all the samples, one at $3,430\text{ cm}^{-1}$ and the other around $1,630\text{ cm}^{-1}$. These correspond to the surface-adsorbed water and oxygen species after calcination [27]. Small characteristic bands of CO_2 chemisorbed on the surface were observed in all the samples in the range $1,460$ – $1,300\text{ cm}^{-1}$. This is reasonable because these are high surface materials. These results are similar for $\text{AFeO}_{3-\delta}$ (A = alkaline earth) prepared by thermal decomposition of alkaline earth nitroprussides [35, 36] and for LnFeO_3 obtained from lanthanide hexacyanoferates (III) precursors [25, 27]. Two strong bands around 587 and 440 cm^{-1} are related to the Fe–O stretching and bending vibrations, respectively, being characteristics of the octahedral FeO_6 groups in perovskite compounds [26, 27].

Figure 6 shows the temperature dependence of the magnetization under both ZFC and FC conditions. At low temperature, an important difference between both curves is observed (Fig. 6). A very similar behavior was observed for

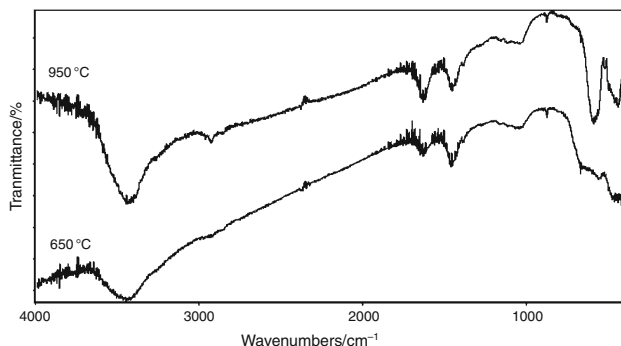


Fig. 5 FTIR spectra for the samples obtained by thermal decomposition of $\text{Y}[\text{Fe}(\text{CN})_6] \cdot 4\text{H}_2\text{O}$ at different temperatures

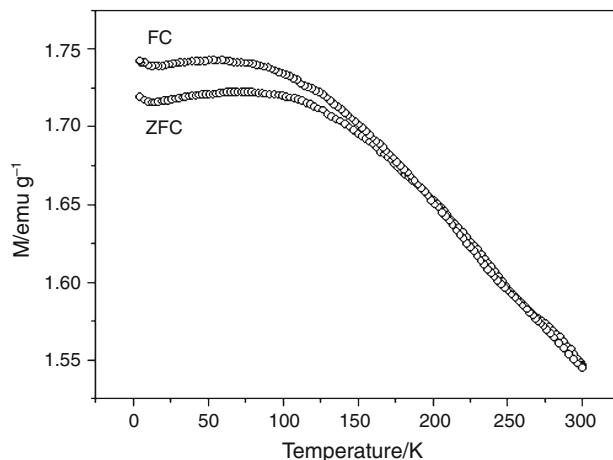


Fig. 6 Temperature dependence of magnetization under zero field-cooled (ZFC) and field-cooled (FC) for orthorhombic YFeO_3

YFeO_3 nanoparticles by Maiti et al. [6]. Unfortunately, the Néel temperature (T_N) of YFeO_3 cannot be observed because it exceeded the temperature range of the equipment. The T_N determined by Shen et al. was 644.5 K [18]. The M–H hysteresis loop at 5 K of YFeO_3 powder prepared at 950 °C is presented in Fig. 7. The coercivity found is about 24 kOe that is in agreement with the value reported by Mathur et al. [20]. The distortion from the ideal perovskite is mainly in the position of the Y^{3+} ions, whereas the Fe^{3+} ions are present in an essentially octahedral environment. Because the alignment of Fe moments is not strictly antiparallel but slightly canted, this results in a small net magnetization, giving rise to a weak ferromagnetic behavior [20].

The size and morphologies of $\text{Y}[\text{Fe}(\text{CN})_6] \cdot 4\text{H}_2\text{O}$ and its decomposition products were investigated by SEM as shown in Fig. 8. The SEM photograph of $\text{Y}[\text{Fe}(\text{CN})_6] \cdot 4\text{H}_2\text{O}$ powder in Fig. 8a shows that it is composed of large well-defined

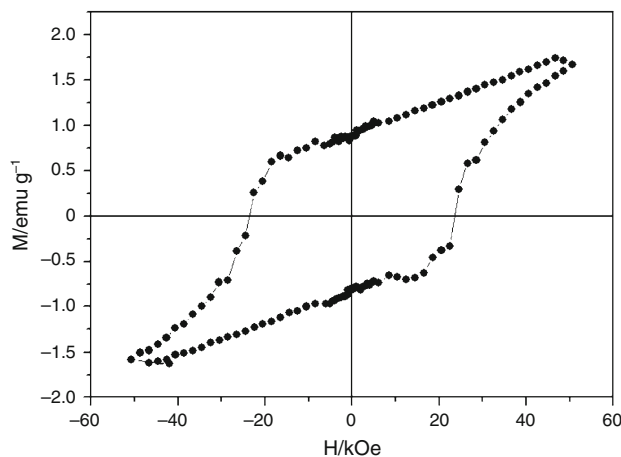


Fig. 7 Hysteresis loop at 5 K for YFeO_3 prepared at 950 °C

crystals with different shapes and with sharp edges up to 3 μm in size. The SEM photograph of hexagonal YFeO₃ obtained at 700 °C (Fig. 8b) clearly shows that the shape and morphology is quite different with that of its precursor complex. The large crystals of the precursor were completely disrupted and extremely fine particles which are loosely aggregated appeared. Because of the extremely small dimensions (on order of 50 nm) and high surface area of the hexagonal YFeO₃ particles, it is easy for them to aggregate as seen in Fig. 8b. Figure 8c shows SEM photograph of

orthorhombic YFeO₃. This image reveals that orthorhombic YFeO₃ is sponge-like and porous agglomerate with pore size of about 0.1 μm . The pores are formed by fast expulsion of gas evolving during the decomposition process.

The atomic proportions of Y, Fe, and O in YFeO₃ determined by EDS are 45.40, 29.60, and 25.17%, respectively. These results show that Y and Fe are present in 1:1 ratio in the residue heated at 950 °C.

Conclusions

In this study, YFeO₃ was successfully synthesized through the thermal decomposition of the Y[Fe(CN)₆]·4H₂O complex as a precursor. The thermal decomposition of Y[Fe(CN)₆]·4H₂O in air was studied using TG/DTA analysis. It decomposes in four steps. The first one corresponds to the elimination of three water molecules loosely bounded (non-coordinated water), the second one to the loss of the remaining water molecule strongly bounded (coordinated water), the third one to the cyanide elimination by combustion to give hexagonal YFeO₃ mixed with Fe₂O₃ and Y₂O₃, and finally in the fourth step (without mass loss) the formation of orthorhombic YFeO₃ as a final product, mixed with a small amount of Y₂O₃.

We refine the structure of the orthorhombic YFeO₃ obtained at 950 °C and found that it was slightly deficient in Y, which is in agreement with the small amount of Y₂O₃ found as an impurity in the sample. The formula of the orthorhombic phase should be written as Y_{0.986}FeO₃, which should indicate a slight oxidation of Fe³⁺ to Fe⁴⁺. YFeO₃ prepared by this method is a canted antiferromagnet with a weak ferromagnetic behavior.

Acknowledgements R.E.C. thanks ANPCYT for PICT2007 303, CONICET for PIP #11220090100995, and SECyT-UNC for Proyecto 159/09. D.M.G. thanks CONICET for a fellowship. D.M.G., M.C.N., and M.I.G. thank CIUNT for financial support.

References

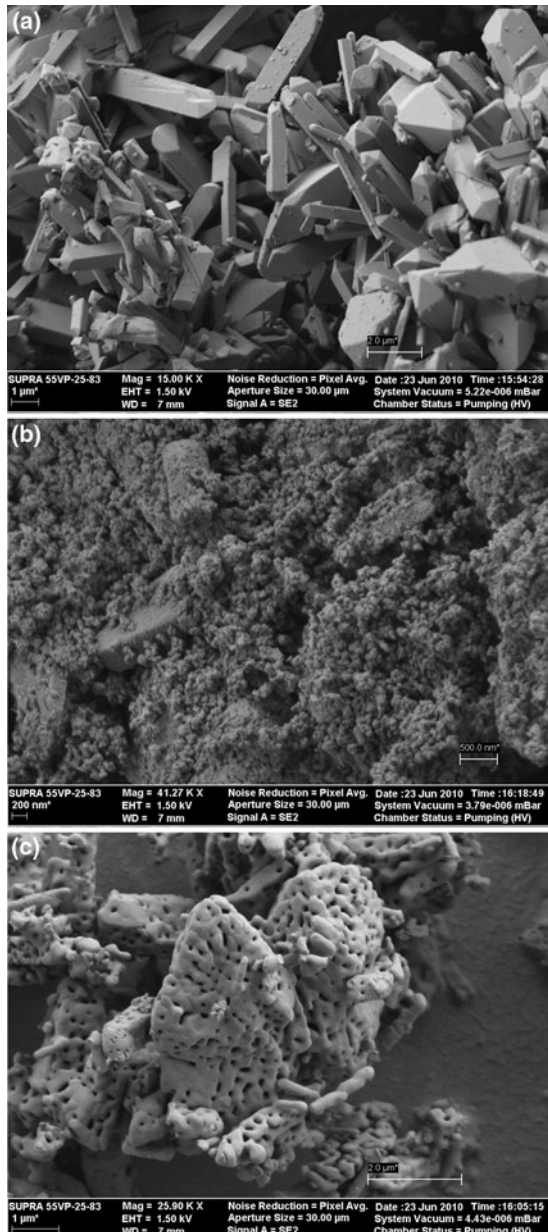


Fig. 8 Scanning electron microscopy of: **a** Y[Fe(CN)₆]·4H₂O, **b** Y[Fe(CN)₆]·4H₂O heated at 700 °C, and **c** Y[Fe(CN)₆]·4H₂O heated at 950 °C

1. Abakumov A, Haderman J, Van Tendeloo G, Antipov E. Chemistry and structure of anion-deficient perovskites with translational interfaces. *J Am Ceram Soc*. 2008;91(6):1807–13.
2. Yuan GL, Or SW, Wang YP, Liu JM. Preparation and multi-properties of insulated single phase BiFeO₃ ceramics. *Solid State Commun*. 2006;138:76–81.
3. Yun KY, Noda M, Okuyama M. Structural and multiferroic properties of BiFeO₃ thin films at room temperature. *J Appl Phys*. 2004;96:3399–403.
4. Moreira dos Santos A, Parashar S, Raju AR, Zhao YS, Cheetham AK, Rao CNR. Evidence for the likely occurrence of magneto-ferroelectricity in the simple perovskite, BiMnO₃. *Solid State Commun*. 2002;122:49–52.
5. Yang CH, Koo TY, Jeong YH. Orbital order, magnetism and ferroelectricity of multiferroic BiMnO₃. *J Magn Magn Mater*. 2007;3:167–70.

6. Maiti R, Basu S, Chakravorty D. Synthesis of nanocrystalline YFeO_3 and its magnetic properties. *J Magn Magn Mater.* 2009;321:3274–7.
7. Yin LH, Song WH, Jiao XL, Wu WB, Li LJ, Tang W, Zhu XB, Yang ZR, Dai JM, Zhang RL, Sun YP. A study of the magnetic and dielectric properties of $\text{YFe}_{0.5}\text{Cr}_{0.5}\text{O}_3$. *Solid State Commun.* 2010;150:1074–6.
8. Yamaguchi O, Takemura H, Yamashita M. Formation of yttrium iron oxides derived from alkoxides. *J Electrochem Soc.* 1991;138:1492–4.
9. Wu L, Yu J, Zhang L, Wang X, Li S. Selective self-propagating combustion synthesis of hexagonal and orthorhombic nanocrystalline yttrium iron oxide. *J Solid State Chem.* 2004;177:3666–74.
10. Du Buolay D, Maslem EN, Streltsov VA, Ishizawa N. A synchrotron X-ray study of the electron density of YFeO_3 . *Acta Cryst.* 1995;B51:921–9.
11. Li J, Singh UG, Schladt TD, Stalick JK, Scott SL, Seshadri R. Hexagonal $\text{YFe}_{1-x}\text{Pd}_x\text{O}_{3-\delta}$: nonperovskite host compound for Pd^{2+} and their catalytic activity for CO oxidation. *Chem Mater.* 2008;20:6567–76.
12. Inoue T, Seki N, Eguchi K, Arai H. Low temperature operation of solid electrolyte oxygen sensors using perovskite type oxide electrodes and cathodic reaction kinetics. *J Electrochem Soc.* 1990;137:2523–7.
13. Alcock CB, Doshi RC, Shen Y. Perovskite electrodes for sensors. *Solid State Ionics.* 1992;51:281–9.
14. Martinelli G, Carotta MC, Ferroni M, Sadaoka Y, Traversa E. Screen-printed perovskite-type thick films as gas sensors for environmental monitoring. *Sens Actuators B.* 1999;55:99–110.
15. Lu X, Xie J, Shu H, Liu J, Yin C, Lin J. Microwave-assisted synthesis of nanocrystalline YFeO_3 and study of its photoactivity. *Mater Sci Eng B.* 2007;138:289–92.
16. Lentmaier J, Kemmler-Sack S, Knell G, Kessler P, Plies P. Selective reduction of nitrogen monoxide by catalysts based on composites between solid acid and perovskite in the presence of excess oxygen. *Mater Res Bull.* 1996;31:1269–76.
17. Lentmaier J, Kemmler-Sack S. Bifunctional YFeO_3 -based catalyst used in the selective catalytic reduction on nitrogen monoxide in the presence of excess of oxygen. *Mater Res Bull.* 1998;33:461–73.
18. Shen H, Xu J, Wu A, Zhao J, Shi M. Magnetic and thermal properties of perovskite YFeO_3 single crystals. *Mater Sci Eng B.* 2009;157:78–80.
19. Dahmani A, Taibi M, Nogues M, Aride J, Loudghiri E, Belayachi A. Magnetic properties of perovskite compounds $\text{YCr}_{1-x}\text{Fe}_x\text{O}_3$ ($0.5 \leq x \leq 1$). *Mater Chem Phys.* 2002;77:912–7.
20. Mathur S, Veith M, Rapalaviciute R, Shen H, Goya G, Martins Filho W, Berquo T. Molecule derived synthesis of nanocrystalline YFeO_3 and investigations on its weak ferromagnetic behavior. *Chem Mater.* 2004;16:1906–13.
21. Samal SL, Green W, Lofland SE, Ramanujachary KV, Das D, Ganguli AK. Study on the solid solution of $\text{YMn}_{1-x}\text{Fe}_x\text{O}_3$: structural, magnetic and dielectric properties. *J Solid State Chem.* 2008;181:61–6.
22. Cristóbal AA, Botta PM, Bercoff PG, Aglietti EF, Bertorello HR, Porto López JM. Mechanochemically assisted synthesis of yttrium-lanthanum orthoferrite: structural and magnetic characterization. *J Alloy Compd.* 2010;495:516–9.
23. Kovachev S, Kovacheva D, Aleksovska S, Svab E, Krezhov K. Structure and magnetic properties of multiferroic $\text{YCr}_{1-x}\text{Fe}_x\text{O}_3$ ($0 \leq x \leq 1$). *J Optoelectron Adv Mater.* 2009;11:1549–52.
24. Sugawara M, Kikukawa N, Ishikawa N, Kayanot N, Kimurat T. Synthesis of Y–Fe–O ultrafine particles using inductively coupled plasma. *J Aerosol Sci.* 1998;5:675–86.
25. Traversa E, Nunziante P, Sakamoto M, Sadaoka Y, Carotta MC, Martinelli G. Thermal evolution of the microstructure of nano-sized LaFeO_3 powders from the thermal decomposition of a heteronuclear complex, $\text{La}[\text{Fe}(\text{CN})_6] \cdot 5\text{H}_2\text{O}$. *J Mater Res.* 1998;13:1335–43.
26. Kondo N, Itoh H, Kurihara M, Sakamoto M, Aono H, Sadaoka Y. New high-yield preparation procedure of $\text{Ln}[\text{Fe}(\text{CN})_6] \cdot n\text{H}_2\text{O}$ ($\text{Ln} = \text{La, Gd, and Lu}$) and their thermal decomposition into perovskite-type oxides. *J Alloy Compd.* 2006;408:1026–9.
27. Navarro MC, Pannunzio-Miner EV, Pagola S, Gómez MI, Carbonio RE. Structural refinement of $\text{Nd}[\text{Fe}(\text{CN})_6] \cdot 4\text{H}_2\text{O}$ and study of NdFeO_3 obtained by its oxidative thermal decomposition at very low temperatures. *J Solid State Chem.* 2005;178:847–54.
28. Masuda Y, Seto Y, Wang X, Yukawa Y, Arii T. A thermal and structural study on lanthanum hexacyanocobaltate (III) pentahydrate, $\text{La}[\text{Co}(\text{CN})_6] \cdot 5\text{H}_2\text{O}$. *J Therm Anal Calorim.* 2000;60:1033–41.
29. Seto Y, Umemoto K, Arii T, Masuda Y. Synthesis and thermal decomposition of lanthanide hexacyanochromate (III) complexes, $\text{Ln}[\text{Cr}(\text{CN})_6] \cdot n\text{H}_2\text{O}$ ($\text{Ln} = \text{La-Lu}; n = 3, 4$). *J Therm Anal Calorim.* 2004;76:165–77.
30. Itagaki Y, Mori M, Hosoya Y, Aono H, Sadaoka Y. O_3 and NO_2 sensing properties of $\text{SmFe}_{1-x}\text{Co}_x\text{O}_3$ perovskite oxides. *Sens Actuators B.* 2007;122:315–20.
31. Medina Córdoba L, Gómez MI, Morán JA, de Aymonino PJ. Synthesis of the $\text{SrFeO}_{2.5}$ and BaFeO_{3-x} perovskites by thermal decomposition of $\text{SrNH}_4[\text{Fe}(\text{CN})_6] \cdot 3\text{H}_2\text{O}$ and $\text{BaNH}_4[\text{Fe}(\text{CN})_6]$. *J Argent Chem Soc.* 2008;96:1–12.
32. Gil DM, Carbonio RE, Gómez MI. Synthesis of $\text{Pb}_2\text{Fe}_2\text{O}_5$ by thermal decomposition of $\text{Pb}_2[\text{Fe}(\text{CN})_6] \cdot 4\text{H}_2\text{O}$. *J Chil Chem Soc.* 2010;55(2):189–92.
33. Navarro MC, Lagarrigue MC, De Paoli JM, Carbonio RE, Gómez MI. A new method of synthesis of BiFeO_3 prepared by thermal decomposition of $\text{Bi}[\text{Fe}(\text{CN})_6] \cdot 4\text{H}_2\text{O}$. *J Therm Anal Calorim.* 2010;102(2):655–60.
34. Farhadi S, Rashidi N. Microwave-induced solid-state decomposition of the $\text{Bi}[\text{Fe}(\text{CN})_6] \cdot 5\text{H}_2\text{O}$ precursor: a novel route for the rapid and facile synthesis of pure and single phase BiFeO_3 nanopowder. *J Alloy Compd.* 2010;503:439–44.
35. Gómez MI, Morán JA, de Carbonio RE, Aymonino PJ. Synthesis of $\text{AFeO}_{2.5+x}$ ($0 \leq x \leq 0.5$; $\text{A} = \text{Sr, Ca}$) mixed oxides from the oxidative thermal decomposition of $\text{A}[\text{Fe}(\text{CN})_5\text{NO}] \cdot 4\text{H}_2\text{O}$. *J Solid State Chem.* 1999;142:138–45.
36. Gómez MI, Lucotti G, Morán JA, Aymonino PJ, Pagola S, Stephens P, Carbonio RE. Ab initio structure solution of $\text{BaFeO}_{2.8-\delta}$, a new polytype in the system BaFeO_3 ($2.5 \leq y \leq 3.0$) prepared from the oxidative thermal decomposition of $\text{Ba}[\text{Fe}(\text{CN})_5\text{NO}] \cdot 3\text{H}_2\text{O}$. *J Solid State Chem.* 2001;160:17–24.
37. Malghe YS, Dharwadkar SR. LaCrO_3 powder from lanthanum trisoxalatochromate (III) precursor, microwave aided synthesis and thermal characterization. *J Therm Anal Calorim.* 2008;91:915–8.
38. Nakayama S, Okazaki M, Aung YL, Sakamoto M. Preparation of perovskite-type oxides LaCoO_3 from three different methods and their evaluation by homogeneity, sinterability and conductivity. *Solid State Ionics.* 2003;158:133–9.
39. Young RA. The Rietveld method. Oxford: Oxford Scientific Publications; 1995.
40. Rodriguez Carbajal J. Determination of the crystallized fractions of a largely amorphous multiphase material by the Rietveld method. *Physica B.* 1993;192:55–69.
41. Finger LW, Cox DE, Jephcoat AP. A correction for powder diffraction peak asymmetry due to axial divergence. *J Appl Cryst.* 1994;27:892–900.
42. Rai D, Danon J. Mossbauer spectroscopic studies of thermal decomposition of alkali ferricyanides. *J Inorg Nucl Chem.* 1975;37:2039–45.

43. Fanning JC, Elrod CD, Franke BS, Melnik JD. Prussian blues from the thermal decomposition of $H_4[Fe(CN)_6]$ and $H_3[Fe(CN)_6]$. *J Inorg Nucl Chem*. 1972;34:139–48.
44. Martinez-Garcia R, Knobel M, Reguera E. Thermal-induced change in molecular magnets based on prussian blue analogues. *J Phys Chem*. 2006;110:7296–303.
45. Gallagher PK, Prescott B. Further studies of the thermal decomposition of Europium hexacyanoferrate (III) and ammonium europium hexacyanoferrate (II). *Inorg Chem*. 1970; 9(11):2510–2.
46. Nakamoto K. Infrared and Raman spectra of inorganic and coordination compounds. New York: Wiley; 1986.
47. Avila M, Reguera L, Rodriguez Hernandez J, Balmaceda J, Reguera E. Porous framework of $T_2[Fe(CN)_6] \cdot xH_2O$ with T=Co, Ni, Cu, Zn and H_2 storage. *J Solid State Chem*. 2008;181: 2899–907.